Science of the Total Environment 659 (2019) 1555–1566

Contents lists available at ScienceDirect

Science of the Total Environment

journal homepage: www.elsevier.com/locate/scitotenv

Characterizing grassland fire activity in the Flint Hills region and air quality using satellite and routine surface monitor data

K.R. Baker [a,*], S.N. Koplitz [a], K.M. Foley [a], L. Avey [b], A. Hawkins [b]

[a] U.S. Environmental Protection Agency, Research Triangle Park, NC, USA
[b] U.S. Environmental Protection Agency, Lenexa, KS, USA

HIGHLIGHTS

- Over half of annual fire detections in the Flints Hills happen in March and April
- Annual acres burned in the area ranges from 0.2 to 2 million acres.
- Up to 38% (14% average) of grassland in the area are burned annually.
- Strongest relationships between $PM_{2.5}$ (carbon and K), O_3, and fire activity

GRAPHICAL ABSTRACT

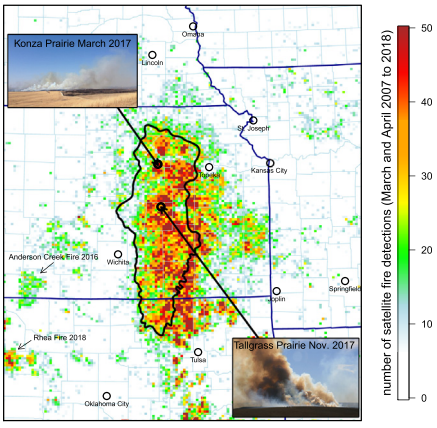

ARTICLE INFO

Article history:
Received 11 October 2018
Received in revised form 28 December 2018
Accepted 28 December 2018
Available online 02 January 2019

Editor: Jianmin Chen

Keywords:
Flint Hills
Grassland
Prescribed fire
Air quality
$PM_{2.5}$
O_3

ABSTRACT

Prescribed grassland fires in the Flint Hills region of central Kansas and northern Oklahoma are a common tool for land management. Local to regional scale impacts on air quality from grassland fires in this region are not well understood, which is important as these types of prescribed fires may increase in the future to preserve broader areas of native grasses in the central U.S. Routine air quality and deposition measurements from sites in and near the Flint Hills were examined for coincident increases during periods of increased prescribed grassland fires. Prescribed fire activity in this region was quantified using satellite detections and multiple publicly available data products of area burned information. March and April comprise over half (41 to 93%) of all annual fire detections in the Flint Hills region seen from satellites between 2007 and 2018 excluding drought years. Annual total fire detections in this region range between 1 and 12 thousand and account for approximately 3% of all fire detections in the contiguous U.S. Annual acres burned ranged from 0.2 to 2 million acres based on U.S. EPA's National Emission Inventory, which accounts for 4 to 38% of grasslands in the area. A comparison of weekly standardized anomalies suggests a relationship between periods of increased grassland fire activity and elevated levels of $PM_{2.5}$ organic carbon, elemental carbon, and potassium. Daily 1-hr maximum ozone (O_3), ammonia (NH_3), sulfur dioxide (SO_2), and oxidized nitrogen gases measured at Konza Prairie also had increased levels when prescribed grassland fire activity was highest. This detailed characterization of prescribed fire activity in the Flint Hills and associated air quality impacts will benefit future efforts to understand changes in atmospheric composition due to changing land management practices.

* Corresponding author.
E-mail address: baker.kirk@epa.gov (K.R. Baker).

https://doi.org/10.1016/j.scitotenv.2018.12.427
0048-9697/

1. Introduction

Wildland fire smoke is known to cause negative health effects in humans (Reid et al., 2016). Further, certain groups are more susceptible to wildland fire smoke exposure which can increase the likelihood of negative health consequences. One of the regions in the U.S. identified as more susceptible due to population traits is central and eastern Kansas (Rappold et al., 2017). Prescribed burning in the Flint Hills region of central Kansas and northern Oklahoma is done to preserve the grassland ecosystem through prevention of woody vegetation encroachment (Towne and Craine, 2016). Reported estimates indicate the Flint Hills region includes over 6 million acres of grassland (Ratajczak et al., 2016; Towne and Craine, 2016) with about half of that burned on a 3 year (or less) cycle to maintain vegetative homogenization (Ratajczak et al., 2016). The most common types of grasses in this region include big bluestem (*Andropogon gerardii*), little bluestem (*Schizachyrium scoparium*), Indian grass (*Sorghastrum nutans*), and cheatgrass (*Bromus tectorum*).

Grassland prescribed fires in this region are typically done each spring season although the amount of acres burned varies from year to year. Variability in burning depends largely on the presence or absence of drought (Mohler and Goodin, 2012). Drought years have less prescribed fire activity due to less vegetation growth and concerns about managing the spread of fire. Economic and cultural factors have led to prescribed burning being done almost exclusively during the spring season, but prescribed burns could be done throughout the year to meet the same ecological and economic goals (Towne and Craine, 2016; Weir and Scasta, 2017). Favorable burn conditions are largely related to minimal recent rainfall (dry fuel) and lower wind speeds that allow for better management of prescribed burns and prevention of uncontrolled spread of fire (Kansas Department of Health and Environment, 2010).

The state of Kansas has used air quality modeling to demonstrate that emissions from grassland burning in the Flint Hills region can contribute to ozone (O_3) levels that exceed the National Ambient Air Quality Standard (NAAQS) in nearby urban areas including Wichita and Kansas City (Kansas Department of Health and Environment, 2012). A state smoke management plan has been developed by Kansas to minimize burning during weather conditions favorable to regional O_3 formation (Kansas Department of Health and Environment, 2010). Grassland burning in the Flint Hills may also impact regional $PM_{2.5}$ monitors, but no formal regulatory contribution demonstrations have been done since this region has been well below the level of the particulate matter less than 2.5 microns ($PM_{2.5}$) NAAQS in recent decades.

Several studies have estimated O_3 and $PM_{2.5}$ impacts from prescribed grassland fires in the Flint Hills. Source attribution statistical models applied to 12 years (2002–2014) of routine speciated $PM_{2.5}$ measurements at Tallgrass Prairie suggest grassland burning during April contributes 42% of average $PM_{2.5}$ for that month at that monitor location (Liu et al., 2016). Statistical analysis of acres burned and ambient O_3 in the Flint Hills region suggests that O_3 levels tend to increase as acres burned increases (Liu et al., 2018). Photochemical grid model simulations of grassland burning in the Flint Hills also show local to regional scale O_3 and $PM_{2.5}$ impacts, although these model simulations were found to systematically overpredict both O_3 and $PM_{2.5}$ from grassland burning in this region (Baker et al., 2016).

Here we build on these previous studies by using multiple satellite fire detection and burned area products to provide more detailed assessments of the spatial patterns of grassland fire activity in the Flint Hills region. We also investigate the temporal variability of prescribed fires in the region across scales (i.e. yearly, weekly, daily, and hourly) to better understand how the size and timing of these fires may be impacting local to regional scale air quality.

Finally, we examine how measurements of a wide range of chemical species made at multiple types of air quality and deposition network monitor locations in and near the Flint Hills vary during periods of increased prescribed fire activity in the region. Our work extends the analysis from previous assessments that focused on a single monitor location in the Flint Hills ecoregion for O_3 (Liu et al., 2018) and speciated $PM_{2.5}$ (Liu et al., 2016) impacts by including more monitor locations and additional pollutants including ammonia, sulfur dioxide (SO_2), carbon dioxide (CO_2), wet deposited species including mercury, and aerosol optical depth (AOD). The goal of this work is to inform future assessments of the air quality impacts of prescribed grassland burning by 1) illustrating which pollutants are most impacted by smoke from prescribed grassland fires in the Flint Hills area, and 2) advancing scientific understanding of how these impacts vary across spatial and temporal scales.

2. Methods

2.1. Fire detections from satellite products

Fire detections are made from geostationary and polar orbiting satellites using both shortwave infrared and visible imagery products made available from the Hazard Mapping System (HMS) (Brey et al., 2017; Hu et al., 2016). Fire detections are included in this analysis from multiple satellites reporting data from 2007 to 2018. Duplicate detections were removed from the dataset when estimating daily totals. All fire detections reported with a method of detection as FDC (Fire Detection and Characterization) were excluded from this analysis to best reflect longer-term trends as this method was introduced as a Geostationary Operational Environmental Satellite (GOES) satellite product in late 2017. The FDC algorithms (https://www.goes-r.gov/education/docs/fs_fire.pdf) reported over twice as many fire detections as all other products combined in 2018 for the contiguous U.S. and the Flint Hills region.

Fire detections may be missed by satellites when masked by clouds (Loría-Salazar et al., 2016) or when the size of the fires is below detection capability (Hu et al., 2016). Fires with short duration outside the overpass window of polar orbiting satellites may also be undetected and not reported. Fire detection analysis suggests prescribed grassland fires in the Flint Hills are often <6 h in duration (Brey et al., 2017), which means these smaller quick burning prescribed grassland fires may be under-reported from polar orbiting satellite products.

2.2. Burned area products

Burned area was totaled for the Flint Hills region and mapped to a common grid structure using multiple sources of data often used to support retrospective and operational smoke modeling. Burned area was extracted from three data sources: the Fire INventory from NCAR (FINN; (Wiedinmyer et al., 2011)), the Global Fire Emission Database (GFED4s; (Van Der Werf et al., 2017)) and U.S. EPA's National Emission Inventory (NEI; (U.S. Environmental Protection Agency, 2018)). FINN estimates global burned area at ~1 km resolution using active fire detections from the Moderate Resolution Imaging Spectroradiometer (MODIS) combined with biomass coverage and fuel type assumptions from the MODIS Vegetation Continuous Fields and Land Cover Type products. GFED4s is also available globally and relies on the MODIS 500 m burned area product (Giglio et al., 2013) supplemented with a small fire parameterization based on MODIS active fire detections (Randerson et al., 2012; Van Der Werf et al., 2017) to produce monthly burned area estimates at ~25 km resolution. Burned area estimates for the contiguous U.S. NEI are produced with the SmartFire v2 system (Raffuse et al., 2012), which reconciles information from multiple sources including ground-based incident reports, fire detections from HMS, and fire perimeters from either the Monitoring Trends in Burned Severity database (MTBS; https://www.mtbs.gov) or the Geospatial Multi-Agency Coordination (GeoMAC; https://www.geomac.gov/index.shtml). Every three years (2008, 2011, 2014, 2017, etc.), the NEI undergoes an iterative evaluation process to include input from state, local, tribal, and other government agencies. For the remaining non-inventory years, estimates of fire activity are still produced with the

SmartFire system, but do not undergo the same iterative review. In this work, we refer to all estimates produced with the SmartFire product as "NEI" including both inventory and non-inventory years.

2.3. Ambient and deposition measurements

Hourly O_3 measurements were obtained from the Clean Air Status and Trends Network (CASTNET; https://www.epa.gov/castnet). CASTNET weekly integrated measurements of SO_2, nitric acid (HNO_3), and $PM_{2.5}$ potassium, chloride, magnesium, sulfate, nitrate, and ammonium were also included in this analysis. Daily averaged $PM_{2.5}$ speciation data was from the Interagency Monitoring of Protected Visual Environments (IMPROVE; http://vista.cira.colostate.edu/Improve/) network and Chemical Speciation Network (CSN; https://www3.epa.gov/ttnamti1/speciepg.html). Two-week integrated ammonia measurements were extracted from the Ammonia Monitoring Network (AMoN; http://nadp.slh.wisc.edu/amon/) (Puchalski et al., 2015). Ambient carbon dioxide measurements were from the AmeriFlux network (http://ameriflux.lbl.gov/).

Ground-based remotely sensed estimates of AOD were obtained from the Aerosol Robotic Network (AERONET; aeronet.gsfc.nasa.gov). Level 1 and 1.5 products were used to minimize potential data exclusion due to prescribed fire smoke misclassified as cloud cover. Weekly total wet deposition and wet concentration of ions was from the National Atmospheric Deposition Program National Trends Network (NTN) (Puchalski et al., 2015) and mercury deposition from the Mercury Deposition Network (MDN) (http://nadp.slh.wisc.edu/). Measured deposited ions include NO_3, SO_4, NH_4, Ca, Na, Mg, K, and Cl.

2.4. Anomaly estimation approach

Although there is a relatively rich set of air quality and fire-related observations in the Flint Hills area that can be used to characterize the air quality impacts of fire emissions, comparing ambient data and fire detections is challenging due to the wide area of potential burning and comparatively sparse surface monitor network (in terms of locations and sampling frequency) meaning winds may not always transport smoke to regional monitor locations and those monitors may not always be sampling on those particular days. Because the different pollutant species span very different ranges of values, measurements were standardized to ease intercomparison and identify common temporal (seasonal) patterns. For a given pollutant concentration $X(s,t)$ at location s and day t, the standardized daily value $X^*(s,t)$ used in this analysis was computed as:

$$X^*(s,t) = \left(X(s,t) - \overline{X}(s)\right)/SD(s),$$

where $\overline{X}(s)$ and $SD(s)$ are the mean and standard deviation, respectively, of $X(s,t)$ across the entire data record at site s. This term is often referred to as the standardized anomaly in long term weather and climatological modeling and data assessments (Wilks, 2006). The daily standardized values were then averaged by week of the year across all available years since 2002 to create an annual profile. Fig. S1 provides the number of observations per week over the entire record of data (Fig. S2) used to support this analysis. The sampling frequency and number of years of data vary by specie. Averaging across these different data records is used to leverage all available data to identify times of the year with increased pollutant concentrations that correspond to increases in fire detection.

2.5. Regression model description

Quantile regression was used to model the relationship between weekly total fire detections from HMS and the weekly average pollutant levels in the Flint Hills area. The model was fit for the 90th percentile pollutant concentrations to quantify how fire activity impacted near-peak pollutant levels. The quantreg library in the R statistical software package (Koenker, 2005) was used to fit the entire time series of year-specific weekly data. Standard error estimates for the slope parameters were fit using the bootstrapping option (i.e. se = "boot" and bsmethod = "xy"). The model was also fit using a subset of the time series focused on the cold season to minimize the influence of summer season O_3 and $PM_{2.5}$ from non-fire sources.

3. Results & discussion

The Flint Hills ecoregion and the extent of the larger area included for fire detections and burned area comparisons are shown in Fig. 1. Grassland and cropland (Fig. S3) landcover is based on the National Land Cover Dataset 2011 (Homer et al., 2015) and shown using 4 km square sized grid cells. There are other large areas of grassland in the central United States outside the Flint Hills area in central Nebraska, southwestern Kansas, and northern Oklahoma. The Flint Hills ecoregion (shown in Fig. 1) covers 6.8 million acres, which includes 4.8 million acres of grassland (5.27 million in the broader area represented by the box) and 1 million acres of cropland based on the U.S. Department of Agriculture 2017 Cropland Data Cover and 2011 National Land Cover Dataset (U.S. Department of Agriculture, 2017). Konza Prairie and Tallgrass Prairie are the only locations in the Flint Hills ecoregion that contribute measurements to routine network monitors. Very few analytes are measured at both locations and none are measured on the same temporal scale.

3.1. Grassland fire activity (fire detections)

Annual total HMS fire detections in the Flint Hills region range from 1.5 thousand in 2013 (drought year) to 12.5 thousand in 2017 with an average of 6.5 thousand between 2007 and 2018 (Table 1). The HMS fire detections in this region typically account for about 3% of all fire detections in the contiguous U.S. and 11% during March and April when activity is highest. In 2014 and 2016 fire detections in the Flint Hills and nearby surrounding areas accounted for 16% of the contiguous U.S. total during the spring.

Fig. 2 shows remotely sensed fire detections in the Flint Hills region by year, month, day of the week, and the percent of detections by hour of the day. Spatial plots of March and April total fire detections by year are provided in Fig. S4 and over all years in the abstract graphic. Grassland fire activity is much higher in March and April compared to the rest of the year and comprises 74 to 93% percent of annual fire detections between 2007 and 2018 excluding the 2013 (41%) drought year (Fig. 2). Fire detections in this region tend to be lowest on Sunday and highest on Saturday. Fire detections from the geostationary GOES satellites show little activity during the nighttime with a steady increase during the morning hours and peak in the early afternoon (Fig. 2). While prescribed fire activity extends throughout the day, individual prescribed grassland fires are typically <6 h (Brey et al., 2017), which means this temporal profile does not provide an indication of start and end time for specific prescribed fires.

The number of fires detected by a specific satellite product varies from year to year and does not always increase or decrease in a similar magnitude with other satellite products (Fig. 2; Table S1). The multi-year analysis of HMS fire detections (Figs. 2, S4, S5) shows that prescribed grassland fires are common features of the landscape in the Flint Hills region each year with some years having less due to drought conditions or weather conditions non-conducive for prescribed burns (e.g., rain, high winds).

3.2. Grassland fire burned area estimates

The number of fires is an indication of activity but estimates of area burned provide an indication about emissions burden for the region. Emissions are a function of emission factors, fuel consumption, and area burned (Larkin et al., 2014). Annual total burned area for the Flint

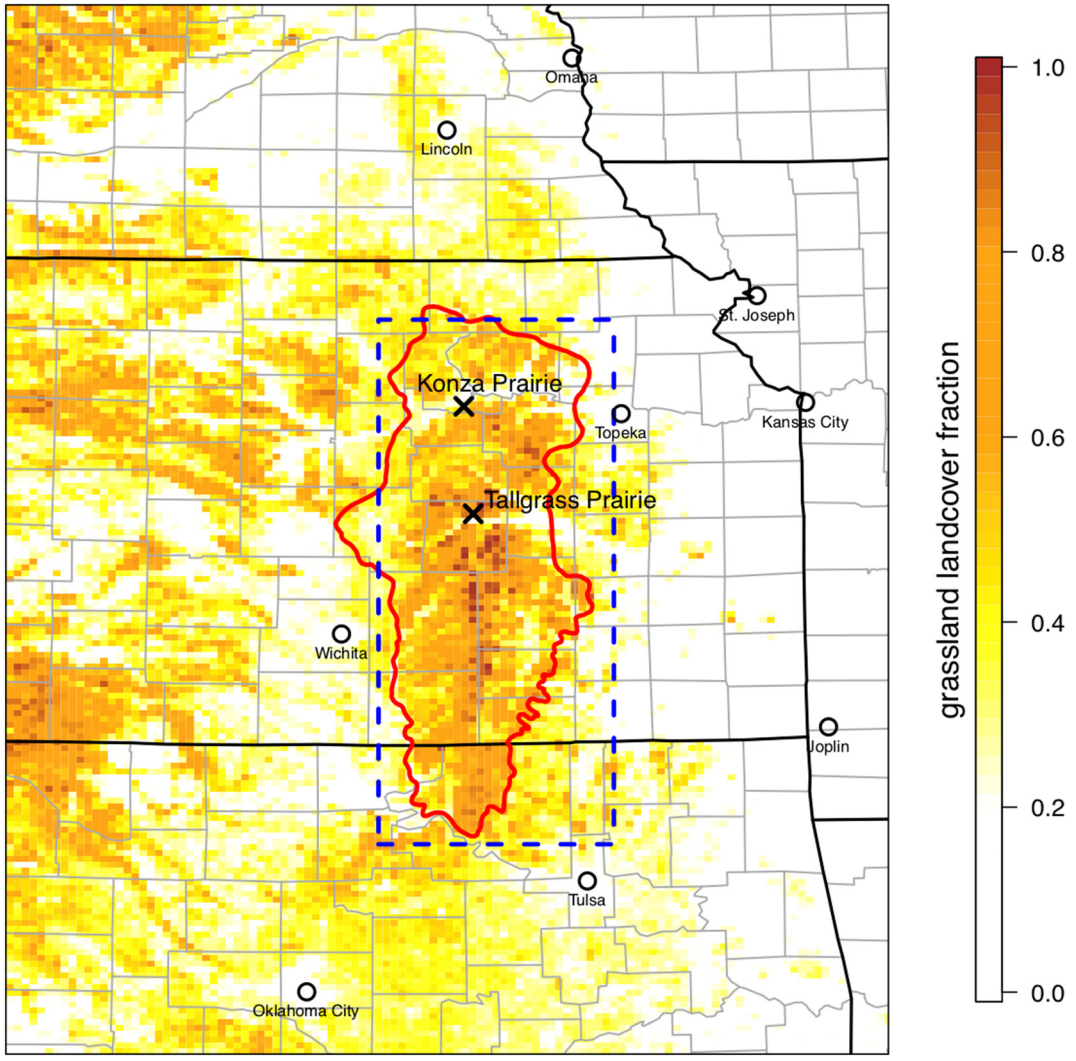

Fig. 1. Grassland shown as a percentage of 4 km square sized cells. The red outline shows the boundary of the Flint Hills ecoregion and the blue box shows the area used for aggregating burn area and fire detections representing the broader Flint Hills area. The Konza Prairie and Tallgrass Prairie monitor locations are also shown. Measurements at each site are indicated in Fig. 5. (For interpretation of the references to colour in this figure legend, the reader is referred to the web version of this article.)

Hills region estimated using multiple data sources is shown in Table 1 and Fig. 3. Annual total acres burned in the Flint Hills region is typically around 800 hundred thousand acres based on the NEI. Over the same time period an average of 6.5 million acres of wildland burned per year in the U.S. (https://www.nifc.gov/fireInfo/fireInfo_stats_totalFires.html).

Annual totals range from 0.03 million acres (2013 drought year GFED product) to 2 million acres (2011 NEI product). The NEI estimated

Table 1
Acres burned and HMS fire detections by year for the Flint Hills area shown in Fig. 1. Acres burned is provided from multiple sources: NEI, GFED, and FINN.

	Burned area (million acres)			Burned area (% of total Flint Hills grassland)			Fire detections	% of all contiguous U.S. fire detections	% of contiguous U.S. fire detections in March and April
Year	NEI	GFED	FINN	NEI	GFED	FINN	HMSH	HMS	HMS
2007	0.5	0.1	0.2	9	2	4	3008	1	6
2008	1.2	0.8	0.4	23	15	8	7130	3	13
2009	0.4	1	0.5	8	19	9	6575	4	11
2010	0.2	0.5	0.4	4	9	8	6927	4	11
2011	2	1.1	0.4	38	21	8	9229	3	11
2012	0.4	0.1	0.1	8	2	2	2762	1	5
2013	0.2	0.03	0.1	4	1	2	1471	1	2
2014	0.9	1.3	0.4	17	25	8	7102	4	16
2015	0.6	0.4	0.3	11	8	6	4769	3	14
2016	1.1	1.1	0.5	21	21	9	9398	5	16
2017							12,460	3	13
2018							7786	2	8
Average	0.8	0.6	0.3	14	12	6	6551	3	11

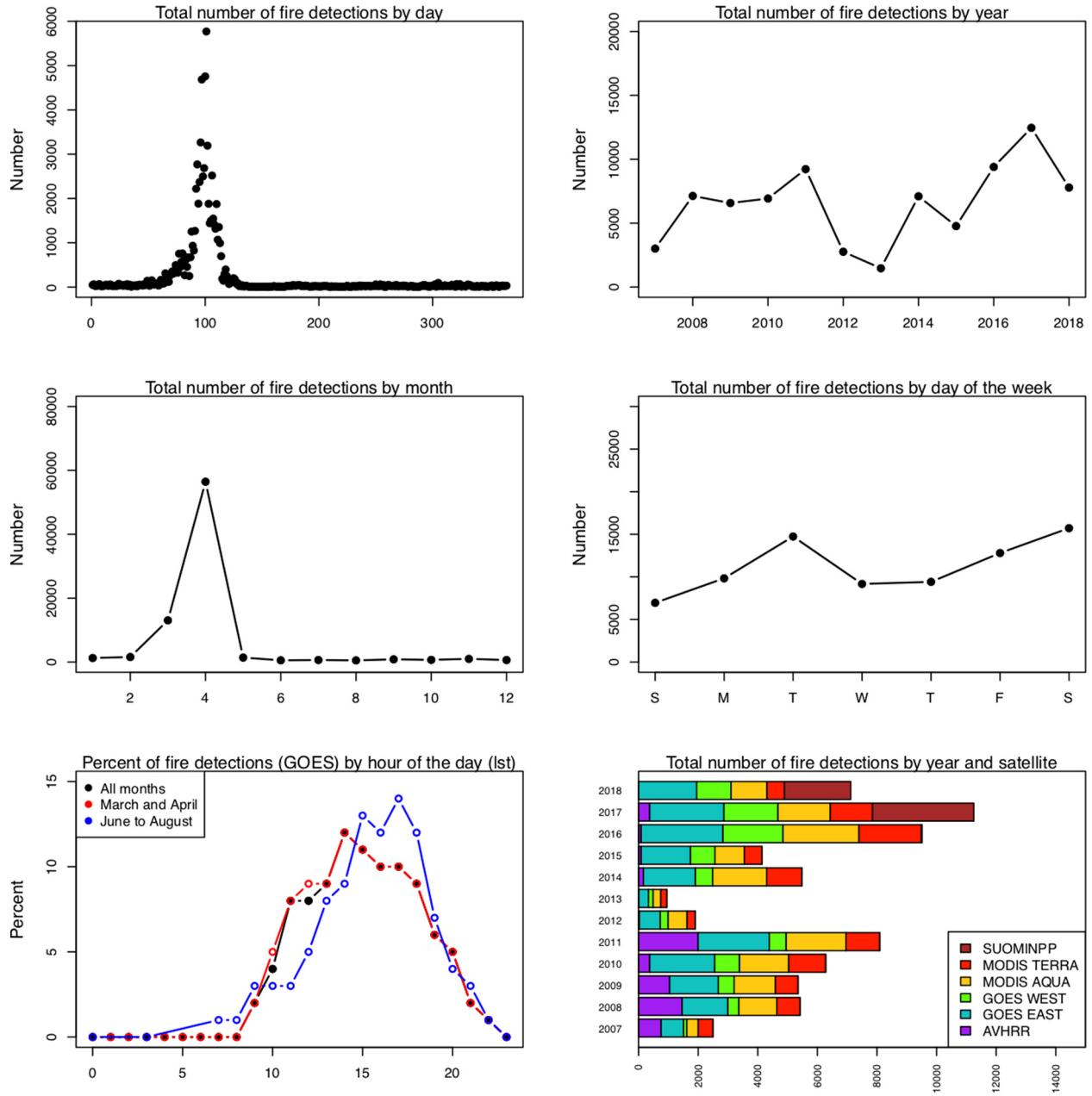

Fig. 2. HMS fire detections for the Flint Hills area between 2007 and 2018 shown by year, month, week, day, and hour (percentage).

annual acres burned is typically about 14% of all grasslands in this area, with a low of 4% and high of 38% in a given year (Table 1). The yearly variation in burn area from these products are similar to values published in literature (Liu et al., 2018), but tend to be lower. Some of the differences with the (Liu et al., 2018) estimate may be related to different methodology for estimating burn area and also extent of area considered in the analysis.

Annual total burned area estimates for this region are similar for the NEI and GFED products while FINN estimates the lowest total for most years. While the NEI and GFED often produce similar total acres burned estimates, the spatial allocation of these burns can be quite different (Fig. 3). The NEI product suggests larger total area burned for 2008 and 2011. These years coincide with the triennial emission inventory process which included additional information and review by agencies augmenting the core set of satellite based information (U.S. Environmental Protection Agency, 2018). Fig. 4 shows NEI estimated total annual area burned as a fraction of the total area of the grid cell (4 square km). Here, total acres burned sometimes exceeds the area of the grid cell which may reflect the simple approach used here for spatial allocation of prescribed fires or an overestimate of some field size assignments. Similar spatial patterns of gridded area burned are evident using FINN (Fig. S6) and GFED (Fig. S7).

Acres burned assigned to specific detected prescribed fires are typically based on default field size assumptions. The median burn area for both NEI and FINN is 150 acres (Fig. 3). Even though the NEI typically assigns similar field sizes as FINN, that method also includes fires assigned specific field sizes that can be much larger. The average burn area in the NEI is 203 acres with many fires exceeding 500 acres (Fig. 3). The NEI estimates of annual total area burned are higher than FINN because of the sometimes much larger burn area assignments and also because FINN only uses fire detections from MODIS whereas NEI uses fire detections from both geostationary and polar orbiting satellites (Koplitz et al., 2018; U.S. Environmental Protection Agency, 2018; Wiedinmyer et al., 2011).

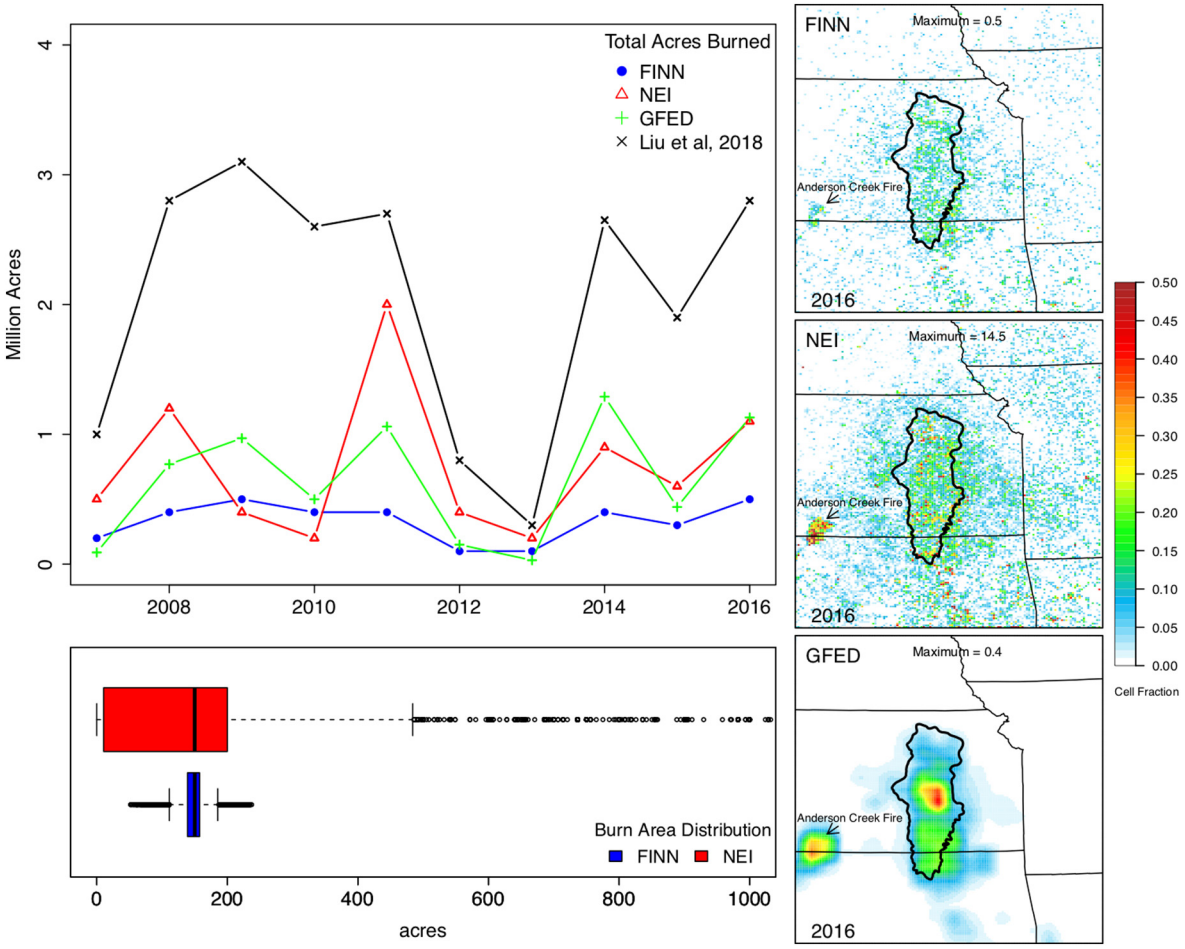

Fig. 3. Annual total burned area estimated for the Flint Hills area using NEI, FINN, and GFED. Annual total estimates are also adapted from Liu et al., 2018, which likely represents a different geographic extent. Gridded total acres burned are shown for 2016 in the right column and the distribution of burn area for specific fires between 2007 and 2016 is shown at bottom left.

Due to its reliance on daily fire detections, FINN is sensitive to missed detections due to cloud cover or other data quality issues which sometimes leads to underestimated burned area during large fires (Paton-Walsh et al., 2012). Conversely, GFED has difficulty capturing small fires, even with the small fire correction in version 4.1s (Koplitz et al., 2018; Reddington et al., 2016). The NEI likely better represents fire activity in the U.S. overall compared to either FINN or GFED since it includes information not used by the global products. Issues related to land cover assumptions and other factors influencing burned area distributions may introduce errors in each of these products (Koplitz et al., 2018; Larkin et al., 2014).

Categorical assignment of fires in this region is important as assignment to wild, prescribed, or cropland will result in differences in emissions model assignment of emission factors, field size assumptions (area burned), allocation of daily emissions to hour of the day, plume rise approach, and speciation of VOC and $PM_{2.5}$ emissions (Baker et al., 2016; Baker et al., 2018; Zhou et al., 2018). Differences in these assignments are important as incorrect assignments can lead to poor model replication of smoke and air quality impacts. Even though prescribed fire in the Flint Hills ecoregion is common, grassland wildfires do occur in the broader area and are evident in the acres burned plots (Fig. 3).

The Anderson Creek wildfire in southwest Kansas and north-central Oklahoma is one of the largest in Kansas history and burned >400,000 acres between March 22 and 31, 2016 (http://wildfiretoday.com/tag/anderson-creek-fire/). This wildfire is clearly evident in both the NEI and GFED burned area products but less pronounced in the FINN burned area product (Fig. 3). This region does not actively manage the grassland with prescribed fire at a scale comparable to the Flint Hills, but local news reports suggest this wildfire was large enough to eliminate some of the woody invasive growth in the region (https://www.kansas.com/news/local/article105463466.html).

3.3. Surface-level ambient speciated particulate matter impacts

Biomass burning directly emits $PM_{2.5}$ and chemical species such as NO_X, SO_2, and NH_3 that are known precursors of secondary $PM_{2.5}$ formation in the atmosphere (Baker et al., 2016; Baker et al., 2018; Wiedinmyer et al., 2011). Previous research has shown local (Liu et al., 2016) to regional scale (Baker et al., 2016) $PM_{2.5}$ impacts from prescribed grassland fire in this region. Springtime increases in $PM_{2.5}$ organic and elemental carbon are evident while sulfate tends to peak in the summer and nitrate during the winter and early spring (Fig. S8).

Fig. 5 shows the average weekly standardized anomaly estimated over all available years of data for pollutants measured at Konza Prairie and Tallgrass Prairie. Table 2 provides quantile regression parameters and significance values for year-specific weekly averaged pollutant levels compared with HMS fire detection totals. The slope parameters in Table 2 are an estimate of the increase in the 90th percentile weekly average pollutant value for every 1000 HMS detects. The corresponding *p*-value indicate whether the estimated slope is statistically significant from zero.

At the Tallgrass Prairie monitor, $PM_{2.5}$ organic carbon ($N = 500$, $\beta = 5.67$, p-value < 0.001), elemental carbon ($N = 500$, $\beta = 1.23$, p-value < 0.001), potassium ($N = 500$, $\beta = 0.19$, p-value < 0.001), chloride ($N = 303$, $\beta = 0.03$, p-value < 0.001), and lead ($N = 500$,

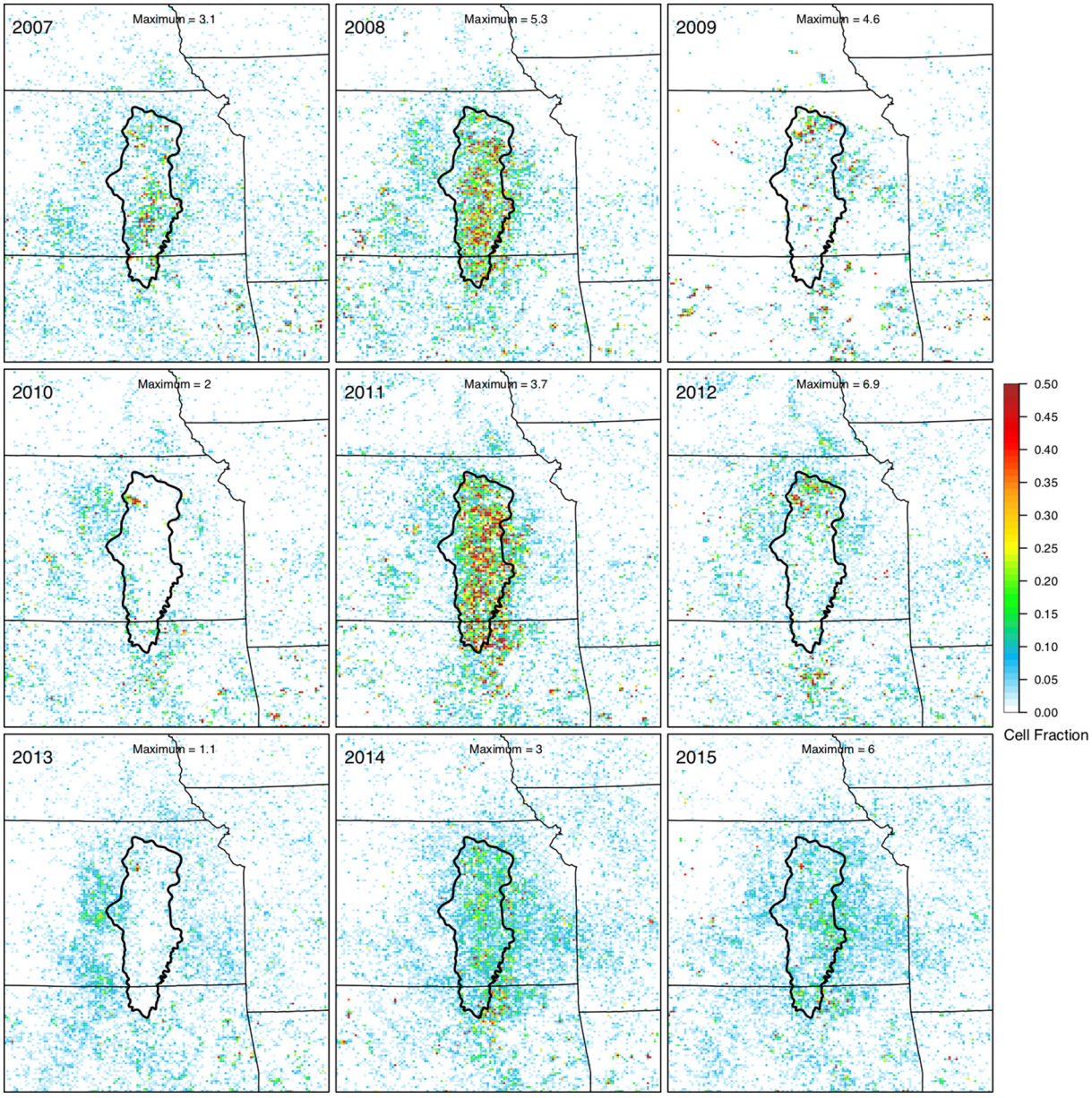

Fig. 4. Total burned area based on the National Emission Inventory approach for March and April for 2007 to 2015 (2016 is shown in Fig. 3).

$\beta = 0.001$, p-value $= 0.1368$) show a strong increase coincident with increased prescribed fire activity in the region while magnesium, silicon, aluminum, iron, copper, and coarse fraction particulate show little or no increase during this time. Similarly, at Konza Prairie, a relationship was evident between prescribed burning activity and $PM_{2.5}$ potassium ($N = 475$, $\beta = 0.10$, p-value < 0.001). Unlike Tallgrass Prairie, a relationship was seen for $PM_{2.5}$ magnesium ($N = 475$, $\beta = 0.01$, p-value $= 0.00124$) while none for chloride. Neither site had a relationship between prescribed fire activity and sulfate, nitrate, calcium, or sodium.

$PM_{2.5}$ sulfate and nitrate do not have a seasonal peak corresponding with fire activity in the Flint Hills region, which suggests other sources dominate contribution to these components of $PM_{2.5}$. However, there are modest increases in precursors SO_2 ($N = 475$, $\beta = 0.19$, p-value $= 0.0028$), ammonia ($N = 95$, $\beta = 1.71$, p-value $= 0.0071$), and nitric acid ($N = 475$, $\beta = 0.80$, p-value $= 0.0015$) at Konza Prairie during the spring season. Ammonia is likely available in the region to convert SO_2 and nitric acid to $PM_{2.5}$ ammonium, so the lack of increased sulfate and nitrate may be due to persistent regional sources of $PM_{2.5}$ sulfate and nitrate overwhelming the contribution from prescribed fires.

The weekly average standardized anomaly at IMPROVE and CSN sites near the Flint Hills region are provided for $PM_{2.5}$ organic carbon (Fig. S9), elemental carbon (Fig. S10), and potassium (Fig. S11) and spatially for the spring season in Fig. 6. Increased $PM_{2.5}$ organic carbon is seen at monitor locations in and near the Flint Hills region during March and April which is when prescribed fire activity is highest. Values are highest at Tallgrass Prairie and Cherokee Nation with an increase also seen downwind in northeast Kansas, western Missouri, and several urban areas including Topeka, KS and Tulsa, OK. It is likely prescribed fires impact other urban monitors in the region but local sources of $PM_{2.5}$ and high levels of $PM_{2.5}$ outside the spring season may obscure impacts of these fires. Other more complex methods such as photochemical modeling would be better suited to differentiate sources of $PM_{2.5}$ in urban areas further downwind of the Flint Hills (Baker et al., 2016).

Many sites with increased spring $PM_{2.5}$ organic carbon anomaly also show a similar increase in $PM_{2.5}$ elemental carbon (Fig. 6). The spatial

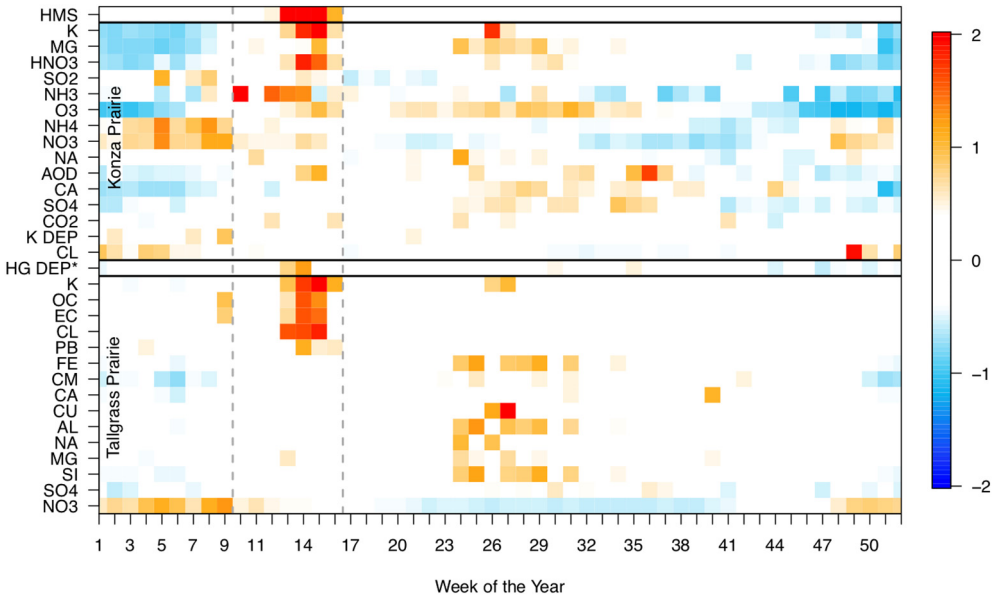

Fig. 5. Average standardized anomaly estimated by week for each measured pollutant. Warm colors indicate levels greater than typical and cool colors represent periods where levels were lower than the long-term average. The number and specific years included for each specie varies (see Fig. S1). Mercury concentration in water (HG DEP) represents 2 monitor locations near the Flint Hills (KS05 and KS31).

pattern of $PM_{2.5}$ potassium in spring is like $PM_{2.5}$ organic and elemental carbon but tends to be less regionally extensive. Potassium is known to be emitted from wildland fire and has been used as a tracer for identifying biomass burning impacts (Li et al., 2003; Liu et al., 2016), but some of the elevated anomaly for potassium is related to other sources. The increased standardized anomaly for $PM_{2.5}$ potassium clearly evident around the Independence Day holiday at all monitor locations (Fig. S11) is reasonable since potassium is a large component of fireworks and elevated potassium has been measured at other locations during holidays (Dickerson et al., 2017). Some of the differences in downwind values for each of these components of $PM_{2.5}$ may also be related to sample frequency differences and which years the monitor operated (Figs. S1 and S2).

Table 2
Quantile regression coefficients for the 90th percentile (tau = 0.9) between year specific weekly average pollutant levels and weekly total HMS fire detections. The regression was applied for the entire data record except for daily 1-hr maximum ozone which excluded the summer season.

Pollutant	Site	N	Units	β1	Pr(>|t|)
$PM_{2.5}$ potassium	Konza	475	μg/m^3	0.10	0.00000
$PM_{2.5}$ magnesium	Konza	475	μg/m^3	0.01	0.00124
Nitric acid	Konza	475	ppb	0.80	0.00152
Sulfur dioxide	Konza	475	ppb	0.19	0.00281
Ammonia	Konza	95	ppb	1.71	0.00717
1-h peak ozone (week <20 or week >40)	Konza	199	ppb	11.37	0.00896
$PM_{2.5}$ ammonium	Konza	475	μg/m^3	−0.13	0.29233
$PM_{2.5}$ nitrate	Konza	475	μg/m^3	0.24	0.44969
$PM_{2.5}$ sodium	Konza	475	μg/m^3	0.02	0.46473
Aerosol optical depth	Konza	64	none	−0.02	0.69579
$PM_{2.5}$ calcium	Konza	475	μg/m^3	0.04	0.78763
$PM_{2.5}$ sulfate	Konza	475	μg/m^3	0.02	0.90588
Carbon dioxide	Konza	270	ppb	−1.27	0.95102
Potassium wet deposition	Konza	343	mg/L	0.008	0.96006
$PM_{2.5}$ chloride	Konza	475	μg/m^3	−0.001	0.96801
Mercury wet deposition	KS05 + KS31	370	ng/L	17.06	0.06772
$PM_{2.5}$ potassium	Tallgrass	500	μg/m^3	0.19	0.00004
$PM_{2.5}$ organic carbon	Tallgrass	500	μg/m^3	5.67	0.00016
$PM_{2.5}$ elemental carbon	Tallgrass	500	μg/m^3	1.23	0.00016
$PM_{2.5}$ chloride	Tallgrass	303	μg/m^3	0.03	0.00073
$PM_{2.5}$ lead	Tallgrass	496	μg/m^3	0.001	0.01368
$PM_{2.5}$ iron	Tallgrass	500	μg/m^3	−0.007	0.06723
Coarse particulate matter	Tallgrass	500	μg/m^3	4.25	0.07682
$PM_{2.5}$ calcium	Tallgrass	500	μg/m^3	0.05	0.15750
$PM_{2.5}$ copper	Tallgrass	496	μg/m^3	0.0001	0.23428
$PM_{2.5}$ aluminum	Tallgrass	493	μg/m^3	−0.011	0.40452
$PM_{2.5}$ sodium	Tallgrass	449	μg/m^3	0.07	0.45584
$PM_{2.5}$ magnesium	Tallgrass	417	μg/m^3	0.005	0.53862
$PM_{2.5}$ silicon	Tallgrass	500	μg/m^3	0.02	0.56814
$PM_{2.5}$ sulfate	Tallgrass	500	μg/m^3	0.25	0.58574
$PM_{2.5}$ nitrate	Tallgrass	500	μg/m^3	0.21	0.75314

3.4. Particulate matter speciation

The relative contribution of different chemical components to total $PM_{2.5}$ from grassland fires is used to support predictive statistical modeling (Liu et al., 2016) and to allocate total $PM_{2.5}$ emissions to specific chemical components for predictive photochemical transport models that simulate wildland fire impacts (Baker et al., 2016). Chemically speciated measurements of $PM_{2.5}$ made at monitor locations in the Flint Hills region where $PM_{2.5}$ organic carbon standardized anomaly exceeds 0.5 during the months of March and April were averaged to generate a composite speciation profile. This threshold resulted in inclusion of 24% of observations at the Tallgrass Prairie and Cherokee Nation monitors combined (Fig. S12). Since sulfate and nitrate ion components were largely regional in nature, these species were assumed to be fully neutralized by ammonium and subtracted from daily total $PM_{2.5}$.

The largest local components of $PM_{2.5}$ mass during periods of increased grassland burning are organic carbon (40%) and elemental carbon (9%) (Fig. 7). Assuming an organic mass to organic carbon ratio of 1.7 (Simon and Bhave, 2011), total organic and elemental carbon related mass account for >85% of local $PM_{2.5}$ during periods of prescribed burning in this area. Fig. 7 also shows the default $PM_{2.5}$ speciation profile used to allocate emissions of total $PM_{2.5}$ to specific chemical constituents used by some modeling systems to estimate smoke impacts (Baker et al., 2016). The distribution of measured fractional composition compares well with the default chemical speciation profile (Simon et al., 2010). Further, the estimate of non-carbon mass associated with organic carbon (NCOM = 0.7 * OC) matched well to the residual estimate shown in Fig. 7 which suggests the bulk of the remaining mass could be explained by organic aerosols. The NCOM consistency with the residual unspeciated mass suggests the mass balance could be closed with NCOM, but this analysis does not definitively show that this mass associated with organic carbon is the unspeciated mass.

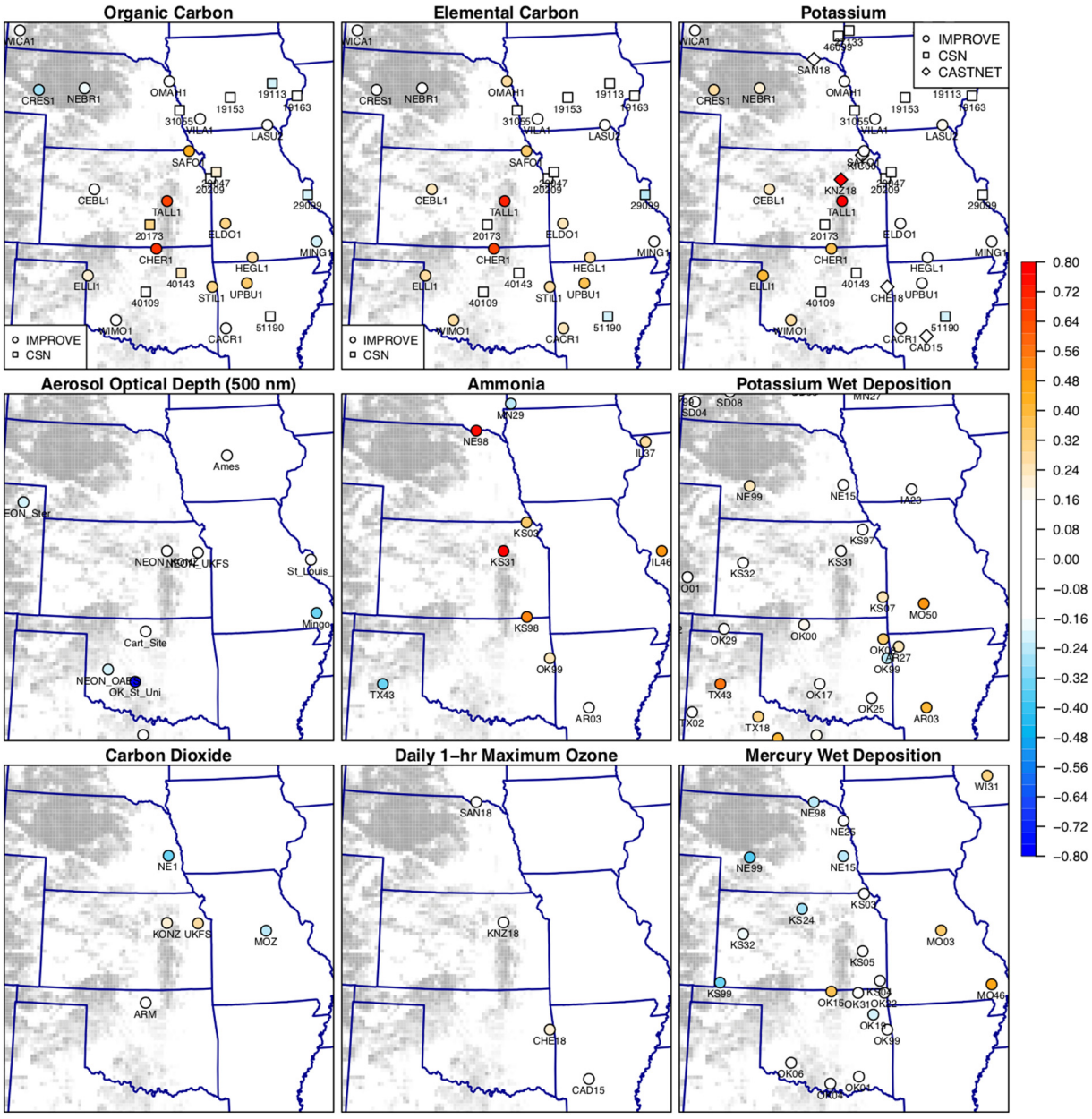

Fig. 6. Week 11 to 16 average standardized anomaly estimated by monitor location for $PM_{2.5}$ organic carbon, $PM_{2.5}$ elemental carbon, $PM_{2.5}$ potassium, aerosol optical depth, ammonia, potassium wet deposition, carbon dioxide, daily 1-h maximum ozone, and mercury wet deposition. Warm colors indicate levels greater than typical and cool colors represent periods where levels were lower than the long-term average. Gray shading indicates grassland landcover.

3.5. Total column particulate matter (aerosol optical depth) impacts

The AOD standardized anomaly at Konza Prairie shows a slight increase during periods of increased spring prescribed burning in the region based on daily maximum AOD (Fig. 5) and no increase in daily average AOD (Fig. S13). Other sites in the region also show no increase in daily average AOD during the spring season. The strong relationship between prescribed fire activity and $PM_{2.5}$ potassium at Konza Prairie suggests the site experiences elevated particulates from regional burning, but these impacts are not evident in the AOD measurement record. This may be due to the presence of clouds impacting AOD retrievals, the lack of data during the spring months at this location (Fig. S14), influence of non-carbon (e.g., sulfate and nitrate) constituents of total $PM_{2.5}$ masking increased AOD levels during the spring season, or some combination of these factors.

3.6. Local (rural) ozone impacts

Biomass burning results in emissions of both NO_X and VOC, which can react in the atmosphere to form O_3 when meteorological conditions (e.g., high temperatures, low wind speeds, and high solar radiation) are favorable (Baker et al., 2016; Baker et al., 2018; Wiedinmyer et al., 2011). A previous study using a statistical model to estimate grassland prescribed fire impacts in the Flint Hills suggests these fires could contribute 12–30 ppb to surface level 8-hr average O_3 levels (Liu et al., 2018). Photochemical modeling studies have indicated a similar range for grassland fires in this region (Baker et al., 2016; Kansas Department of Health and Environment, 2012), but these models have a systematic tendency of over-estimation at monitors predicted to have fire impacts (Baker et al., 2016; Baker et al., 2018).

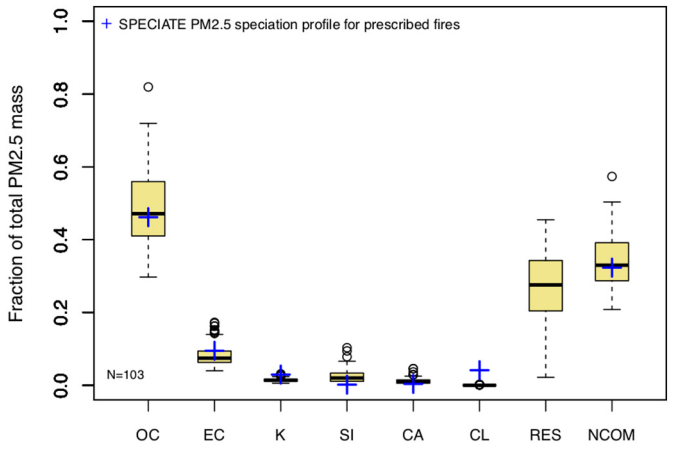

Fig. 7. The distribution of $PM_{2.5}$ chemical components of all samples in the months of March and April where organic carbon standardized anomaly was higher than 0.5 at multiple IMPROVE monitors: Tallgrass Prairie and Cherokee Nation. $PM_{2.5}$ sulfate and nitrate were subtracted from the total mass before normalizing individual components. NCOM was estimated as 0.7*OC. RES is the difference between total $PM_{2.5}$ and the sum of organic carbon (OC), elemental carbon (EC), potassium (K), silicon (SI), calcium (CA), and chloride (CL).

The distribution of O_3 levels at the Konza Prairie and Cherokee Nation monitors are shown by month and week of the year in Fig. 8. The Cherokee Nation site shows a slight increase in median and interquartile O_3 levels during April compared to March and May. Levels at the Konza Prairie site do not suggest a larger interquartile range compared to March and May but do show an increased occurrence of high O_3 levels that are above the interquartile range (Fig. 8). The weekly standardized anomaly of daily maximum 1-hr O_3 at Konza Prairie increases in the spring and is generally coincident with increased prescribed burning in the region (Fig. 5). This increased spring anomaly is physically discontinuous from the elevated summer season O_3 at this monitor location. The relationship between maximum 1-hr O_3 levels and prescribed fire activity (HMS fire detections) is weak when considering the entire year at Konza Prairie but becomes much stronger when excluding the summer season ($N = 199$, $\beta = 11.37$, p-value $= 0.0089$).

Directly relating elevated O_3 levels with increased prescribed fire is challenging since O_3 formation is complicated and requires specific meteorological conditions that are not always present in this region when burning activity is highest. Cool temperatures and high winds are common in the spring, which are not conducive to O_3 formation. Additionally, cloudy conditions common during the spring also inhibit photolytic reactions that can lead to O_3 formation when NO_X and VOC emissions are present (Baker et al., 2016).

3.7. Ammonia impacts

Ammonia is known to be emitted during biomass burning (Wiedinmyer et al., 2011). Several studies suggest increased surface level ammonia is sometimes associated with wildfire (Benedict et al., 2017; Chen et al., 2014; Saylor et al., 2015), but local to regional scale impacts on air quality are not well characterized and no information is available specific to grassland burning impacts near the Flint Hills.

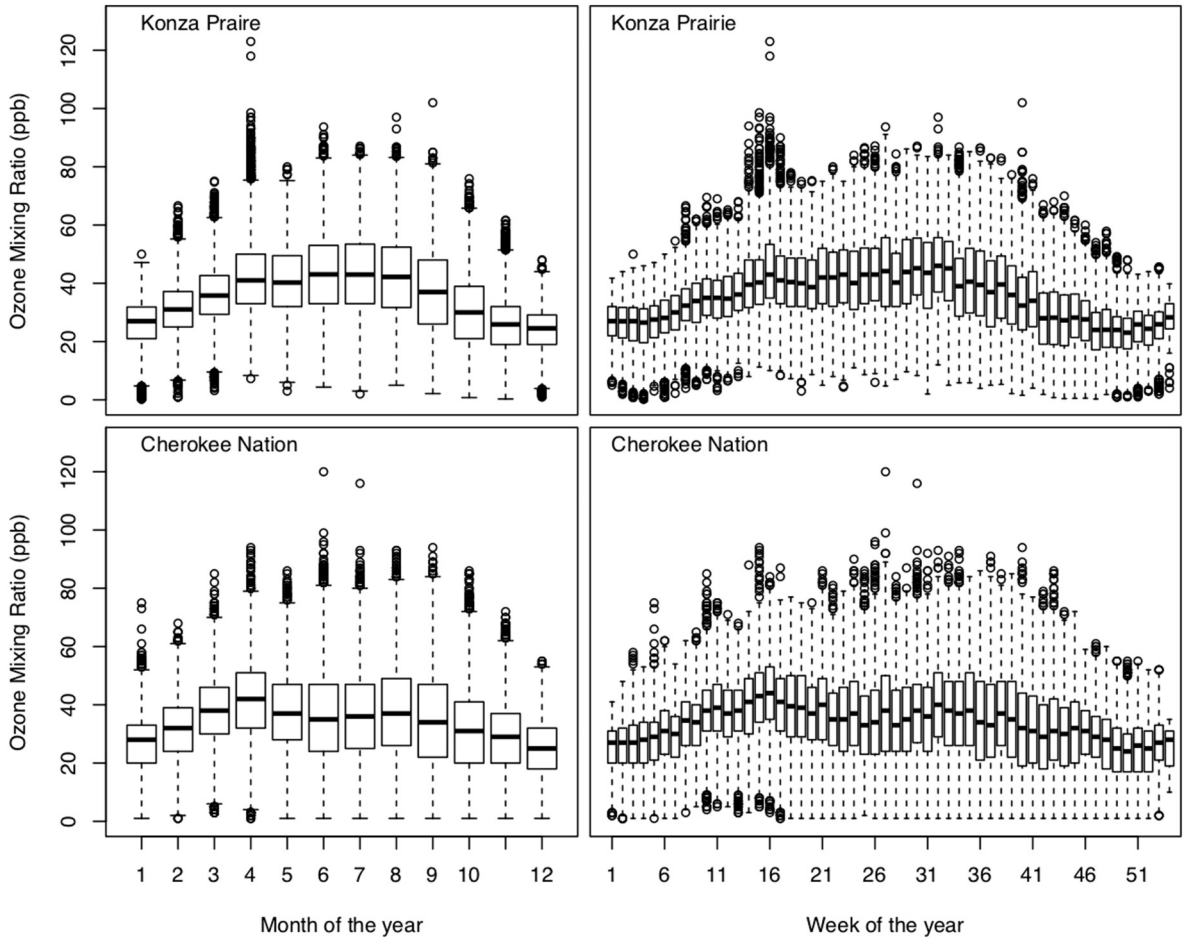

Fig. 8. Distribution of hourly O_3 shown by month (left column) and week of the year (right column) at Konza Prairie (top row) and Cherokee Nation (bottom row). Locations shown in Fig. 6.

The Konza Prairie monitor measuring 2-week integrated ammonia shows a relationship with prescribed grassland burning activity ($N = 95, \beta = 1.71$, p-value = 0.0072) (Table 2). Increased springtime anomalies are seen at Konza Prairie (Fig. 4) and other sites in Kansas, Oklahoma, and Nebraska (Fig. 5). However, these increased anomalies extend into the early summer suggesting other sources may also be contributing to ammonia at these locations (Fig. S15), such as agricultural fertilizer application or the seasonal introduction of additional livestock for grazing in the nearby pasture lands.

3.8. Wet deposition impacts

Mercury has been measured in wildfire plumes. Emissions vary by fuel type and grassland emissions of mercury are substantially lower than trees (Wiedinmyer and Friedli, 2007). Total mercury deposition peaks outside the period of intensive prescribed fire in the region, but mercury concentration in deposited water shows occasional peaks during this period (Fig. S16). The weekly standardized anomaly for multiple sites in the region suggest a modest increase in mercury deposition during the time of increased prescribed grassland fires in the region ($N = 370, \beta = 17$, p-value = 0.067) (Fig. 5; Table 2).

Mercury concentration in wet deposition at monitors near and downwind the Flint Hills region show an increase during the spring season at sites in eastern Kansas (Fig. 6). While many sites have small or negative average mercury deposition standardized anomalies during the spring, most sites downwind of the Flint Hills have one or two weeks (Fig. S17) with a positive anomaly which suggests sites may sometimes be impacted by prescribed grassland fire when weather systems favor transport from the Flint Hills to the monitor and precipitation occurs.

Most mercury emissions from biomass burning are in the form of gaseous elemental mercury which has a long atmospheric lifetime meaning impacts from this form would be regional to continental in scale (Baker and Bash, 2012). A smaller fraction of the emissions are particulate mercury (Wiedinmyer and Friedli, 2007) and this form of mercury may be contributing to local and regional scale deposition as it will be removed from the atmosphere at time scales similar to other chemical forms of particulate matter like organic and elemental carbon (Baker and Bash, 2012).

The distribution of the concentration of wet deposited ions does not show obvious increases during the spring (Fig. S18). Measurements of potassium in wet deposition sometimes show an increased anomaly during March and April (Fig. S19) but not the consistent increase seen for ambient $PM_{2.5}$ potassium (or organic and elemental carbon). In fact, wet deposition anomalies for potassium during the spring are highest in the Ozarks region rather than Flint Hills (Fig. 6). A strong relationship is less likely for wet deposited ions since both prescribed fire and rainfall is needed for an increase to be realized in the monitor data. Rainfall is unlikely given the type of weather conditions (e.g., low winds and no precipitation) associated with prescribed fire. A link between deposited nutrients and wildfire has been seen in other regions of the world (Ponette-González et al., 2016) but no specific studies have shown a relationship between deposited ions and wildland fire in the U.S.

3.9. Impacts on other pollutants

Biomass burning of grasses are known to emit CO_2 (Clements et al., 2006; Strand et al., 2016), but local to regional scale impacts from grassland burning are less well known. Ambient CO_2 levels at monitors in the region do not show large increases during the spring season, even at the Konza Prairie site that is very close to prescribed fire activity (Table 2; Fig. S20). Daily maximum CO_2 standardized anomaly at both Kansas monitor locations show a modest increase during the spring (Fig. 5) while monitors further from the Flint Hills show a negative anomaly over the same timeframe (Fig. S21). Interestingly, the monitor in eastern Kansas (UKFS) shows an increased springtime anomaly for CO_2 but does not show a similar increased anomaly for AOD (Fig. 6).

Biomass burning is known to emit other pollutants into the atmosphere that have negative impacts on human health either directly, indirectly through chemical transformation, or both. Pollutants including CO, VOC, and NO_X are emitted from wildland fire (Benedict et al., 2017; Wiedinmyer et al., 2011) but no measurements were available in the region to provide information about whether prescribed grassland fires may be contributing to the ambient burden. Weekly integrated nitric acid measurements at Konza Prairie show an increase in concentration during the period of prescribed fires in the region, which may be an indirect measure of NO_X but a direct relationship is not clear since in-plume measurements from multiple wildfires (Baker et al., 2018; Cai et al., 2016) suggest peroxyacetyl nitrate (PAN) and not nitric acid is formed in smoke plumes.

4. Implications

Grassland burning in the Flint Hills region is typically comprised of many prescribed fires of short duration during March and April. Ambient measurements of $PM_{2.5}$ constituents including organic carbon, elemental carbon, potassium, chloride, sulfur dioxide, oxidized nitrogen gases, lead, ammonia, and peak 1-hr non-summer season O_3 were elevated during periods of prescribed fire activity in the Flint Hills. The air quality impacts from Flint Hills prescribed fire activity shown here and in previous work represent only one of the many environmental considerations important for land managers in this region. Recent research suggests that extending the burn season outside of the short time period in early April would result in the same ecological benefits for the native grassland ecosystem and promote grass growth for cattle grazing (Weir and Scasta, 2017).

A longer prescribed burning period would allow land managers to meet acres burned goals and potentially allow for larger amounts of annual acres burned in the Flint Hills while decreasing the short-term elevated pollution impacts due to smoke (Towne and Craine, 2016; Weir and Scasta, 2017). Increased burning outside of spring could also allow the region to maintain the cycle of burning (<3 years) needed to minimize invasive woody growth in the region during years when spring time weather may not be conducive for prescribed fire (Ratajczak et al., 2016). More research is needed to better understand the trade-offs of increased prescribed fire activity outside the spring season in the Flint Hills region to help managers optimize land management strategies that also minimize air quality and public health impacts.

Supplementary data

Additional information about fire detections and air quality impacts are provided in the supporting information. Supplementary data to this article can be found online at https://doi.org/10.1016/j.scitotenv.2018.12.427.

Acknowledgements

The authors would like to recognize the contributions of Sean Woznicki, James Beidler, George Pouliot, Jeff Vukovich, Barron Henderson, Heather Simon, Chris Misenis, Ben Gibson, and Lara Reynolds. The National Ecological Observatory Network is a program sponsored by the National Science Foundation and operated under cooperative agreement by Battelle Memorial Institute.

Disclaimer

The views expressed in this article are those of the authors and do not necessarily represent the views or policies of the U.S. Environmental Protection Agency.

References

Baker, K.R., Bash, J.O., 2012. Regional scale photochemical model evaluation of total mercury wet deposition and speciated ambient mercury. Atmos. Environ. 49, 151–162.

Baker, K., Woody, M., Tonnesen, G., Hutzell, W., Pye, H., Beaver, M., Pouliot, G., Pierce, T., 2016. Contribution of regional-scale fire events to ozone and $PM_{2.5}$ air quality estimated by photochemical modeling approaches. Atmos. Environ. 140, 539–554.

Baker, K., Woody, M., Valin, L., Szykman, J., Yates, E., Iraci, L., Choi, H., Soja, A., Koplitz, S., Zhou, L., 2018. Photochemical model evaluation of 2013 California wild fire air quality impacts using surface, aircraft, and satellite data. Sci. Total Environ. 637, 1137–1149.

Benedict, K.B., Prenni, A.J., Carrico, C.M., Sullivan, A.P., Schichtel, B.A., Collett Jr., J.L., 2017. Enhanced concentrations of reactive nitrogen species in wildfire smoke. Atmos. Environ. 148, 8–15.

Brey, S.J., Ruminski, M., Atwood, S.A., Fischer, E.V., 2017. Connecting smoke plumes to sources using hazard mapping system (HMS) smoke and fire location data over North America. Atmos. Chem. Phys. Discuss. https://doi.org/10.5194/acp-2017-245 (in review).

Cai, C., Kulkarni, S., Zhao, Z., Kaduwela, A.P., Avise, J.C., DaMassa, J.A., Singh, H.B., Weinheimer, A.J., Cohen, R.C., Diskin, G.S., 2016. Simulating reactive nitrogen, carbon monoxide, and ozone in California during ARCTAS-CARB 2008 with high wildfire activity. Atmos. Environ. 128, 28–44.

Chen, X., Day, D., Schichtel, B., Malm, W., Matzoll, A.K., Mojica, J., McDade, C.E., Hardison, E.D., Hardison, D.L., Walters, S., 2014. Seasonal ambient ammonia and ammonium concentrations in a pilot IMPROVE NHx monitoring network in the western United States. Atmos. Environ. 91, 118–126.

Clements, C.B., Potter, B.E., Zhong, S., 2006. In situ measurements of water vapor, heat, and CO_2 fluxes within a prescribed grass fire. Int. J. Wildland Fire 15, 299–306.

Dickerson, A.S., Benson, A.F., Buckley, B., Chan, E.A., 2017. Concentrations of individual fine particulate matter components in the USA around July 4th. Air Qual. Atmos. Health 10, 349–358.

Giglio, L., Randerson, J.T., van der Werf, G.R., 2013. Analysis of daily, monthly, and annual burned area using the fourth-generation global fire emissions database (GFED4). J. Geophys. Res. Biogeosci. 118, 317–328.

Homer, C., Dewitz, J., Yang, L., Jin, S., Danielson, P., Xian, G., Coulston, J., Herold, N., Wickham, J., Megown, K., 2015. Completion of the 2011 national land cover database for the conterminous United States–representing a decade of land cover change information. Photogramm. Eng. Remote. Sens. 81, 345–354.

Hu, X., Yu, C., Tian, D., Ruminski, M., Robertson, K., Waller, L.A., Liu, Y., 2016. Comparison of the hazard mapping system (HMS) fire product to ground-based fire records in Georgia, USA. J. Geophys. Res.-Atmos. 121, 2901–2910.

Kansas Department of Health and Environment, 2010. State of Kansas Flint Hills Smoke Management Plan December, 2010. http://www.ksfire.org/docs/about/Flint_Hills_SMP_v10FINAL.pdf.

Kansas Department of Health and Environment, 2012. State of Kansas Exceptional Event Demonstration Package April 6, 12, 13, and 29, 2011. Department of Health and Environment, Division of Environment, Bureau of Air November 27, 2012. http://www.epa.gov/ttn/analysis/docs/KDHE_ExEvents_final_042011.pdf.

Koenker, R.W., 2005. Quantile Regression. Cambring University Press.

Koplitz, S.N., Nolte, C.G., Pouliot, G.A., Vukovich, J.M., Beidler, J., 2018. Influence of uncertainties in burned area estimates on modeled wildland fire $PM_{2.5}$ and ozone pollution in the contiguous US. Atmos. Environ. 191, 328–339.

Larkin, N.K., Raffuse, S.M., Strand, T.M., 2014. Wildland fire emissions, carbon, and climate: US emissions inventories. For. Ecol. Manag. 317, 61–69.

Li, J., Pósfai, M., Hobbs, P.V., Buseck, P.R., 2003. Individual aerosol particles from biomass burning in southern Africa: 2, compositions and aging of inorganic particles. J. Geophys. Res.-Atmos. 108.

Liu, Z., Liu, Y., Maghirang, R., Devlin, D., Blocksome, C., 2016. Estimating contributions of prescribed rangeland burning in Kansas to ambient $PM_{2.5}$ through source apportionment with the Unmix receptor model. Trans. ASABE 59, 1267–1275.

Liu, Z., Liu, Y., Murphy, J.P., Maghirang, R., 2018. Contributions of Kansas rangeland burning to ambient O_3: analysis of data from 2001 to 2016. Sci. Total Environ. 618, 1024–1031.

Loría-Salazar, S.M., Holmes, H.A., Arnott, W.P., Barnard, J.C., Moosmüller, H., 2016. Evaluation of MODIS columnar aerosol retrievals using AERONET in semi-arid Nevada and California, USA, during the summer of 2012. Atmos. Environ. 144, 345–360.

Mohler, R.L., Goodin, D.G., 2012. Mapping burned areas in the Flint Hills of Kansas and Oklahoma, 2000—2010. Great Plains Res. 15–25.

Paton-Walsh, C., Emmons, L.K., Wiedinmyer, C., 2012. Australia's black Saturday fires–comparison of techniques for estimating emissions from vegetation fires. Atmos. Environ. 60, 262–270.

Ponette-González, A.G., Curran, L.M., Pittman, A.M., Carlson, K.M., Steele, B.G., Ratnasari, D., Weathers, K.C., 2016. Biomass burning drives atmospheric nutrient redistribution within forested peatlands in Borneo. Environ. Res. Lett. 11, 085003.

Puchalski, M.A., Rogers, C.M., Baumgardner, R., Mishoe, K.P., Price, G., Smith, M.J., Watkins, N., Lehmann, C.M., 2015. A statistical comparison of active and passive ammonia measurements collected at clean air status and trends network (CASTNET) sites. Environ. Sci.: Processes Impacts 17, 358–369.

Raffuse, S., Du, Y., Larkin, N., Lahm, P., 2012. Development of the 2008 Wildland Fire National Emissions Inventory, 20th International Emissions Inventory Conference, August. pp. 13–16.

Randerson, J., Chen, Y., Werf, G., Rogers, B., Morton, D., 2012. Global burned area and biomass burning emissions from small fires. J. Geophys. Res. Biogeosci. 117.

Rappold, A.G., Reyes, J., Pouliot, G., Cascio, W.E., Diaz-Sanchez, D., 2017. Community vulnerability to health impacts of wildland fire smoke exposure. Environ. Sci. Technol. 51, 6674–6682.

Ratajczak, Z., Briggs, J.M., Goodin, D.G., Luo, L., Mohler, R.L., Nippert, J.B., Obermeyer, B., 2016. Assessing the potential for transitions from tallgrass prairie to woodlands: are we operating beyond critical fire thresholds? Rangel. Ecol. Manag. 69, 280–287.

Reddington, C.L., Spracklen, D.V., Artaxo, P., Ridley, D.A., Rizzo, L.V., Arana, A., 2016. Analysis of particulate emissions from tropical biomass burning using a global aerosol model and long-term surface observations. Atmos. Chem. Phys. 16, 11083–11106.

Reid, C.E., Brauer, M., Johnston, F.H., Jerrett, M., Balmes, J.R., Elliott, C.T., 2016. Critical review of health impacts of wildfire smoke exposure. Environ. Health Perspect. 124, 1334.

Saylor, R., Myles, L., Sibble, D., Caldwell, J., Xing, J., 2015. Recent trends in gas-phase ammonia and $PM_{2.5}$ ammonium in the southeast United States. J. Air Waste Manage. Assoc. 65, 347–357.

Simon, H., Bhave, P.V., 2011. Simulating the degree of oxidation in atmospheric organic particles. Environ. Sci. Technol. 46, 331–339.

Simon, H., Beck, L., Bhave, P.V., Divita, F., Hsu, Y., Luecken, D., Mobley, J.D., Pouliot, G.A., Reff, A., Sarwar, G., 2010. The development and uses of EPA's speciate database. Atmos. Pollut. Res. 1, 196–206.

Strand, T., Gullett, B., Urbanski, S., O'Neill, S., Potter, B., Aurell, J., Holder, A., Larkin, N., Moore, M., Rorig, M., 2016. Grassland and forest understorey biomass emissions from prescribed fires in the south-eastern United States–RxCADRE 2012. Int. J. Wildland Fire 25, 102–113.

Towne, E.G., Craine, J.M., 2016. A critical examination of timing of burning in the Kansas Flint Hills. Rangel. Ecol. Manag. 69, 28–34.

U.S. Department of Agriculture, 2017. USDA National Agricultural Statistics Service Cropland Data Layer. Published Crop-specific Data Layer. USDA-NASS, Washington, DC Available at. https://nassgeodata.gmu.edu/CropScape/, Accessed date: 18 December 2018.

U.S. Environmental Protection Agency, 2018. 2014 National Emissions Inventory, Version 2 Technical Support Document. https://www.epa.gov/sites/production/files/2018-07/documents/nei2014v2_tsd_05jul2018.pdf.

Van Der Werf, G.R., Randerson, J.T., Giglio, L., Van Leeuwen, T.T., Chen, Y., Rogers, B.M., Mu, M., Van Marle, M.J., Morton, D.C., Collatz, G.J., 2017. Global Fire Emissions Estimates During 1997–2016.

Weir, J.R., Scasta, J.D., 2017. Vegetation responses to season of fire in tallgrass prairie: a 13-year case study. Fire Ecol. 13, 137–142.

Wiedinmyer, C., Friedli, H., 2007. Mercury emission estimates from fires: an initial inventory for the United States. Environ. Sci. Technol. 41, 8092–8098.

Wiedinmyer, C., Akagi, S., Yokelson, R.J., Emmons, L., Al-Saadi, J., Orlando, J., Soja, A., 2011. The Fire INventory from NCAR (FINN): a high resolution global model to estimate the emissions from open burning. Geosci. Model Dev. 4, 625.

Wilks, D.S., 2006. Statistical Methods in the Atmospheric Sciences. International Geophysics Series V. 91. Academic Press.

Zhou, L., Baker, K.R., Napelenok, S.L., Pouliot, G., Elleman, R., O'Neill, S.M., Urbanski, S.P., Wong, D.C., 2018. Modeling crop residue burning experiments to evaluate smoke emissions and plume transport. Sci. Total Environ. 627, 523–533.